Nuclear Instruments and Methods in Physics Research B 318 (2014) 19–22

Contents lists available at ScienceDirect

Nuclear Instruments and Methods in Physics Research B

journal homepage: www.elsevier.com/locate/nimb

L-shell X-ray production cross sections induced by protons and alpha-particles in the 0.7–2.0 MeV/amu range for Ru and Ag

A.P.L. Bertol [a,*], J. Trincavelli [b,c], R. Hinrichs [d], M.A.Z. Vasconcellos [a]

[a] Instituto de Física, Universidade Federal do Rio Grande do Sul, Porto Alegre, RS, Brazil
[b] Facultad de Matemática, Astronomía y Física, Universidad Nacional de Córdoba, Argentina
[c] Instituto Enrique Gaviola, CONICET, Argentina
[d] Instituto de Geociências, UFRGS, Porto Alegre, RS, Brazil

ARTICLE INFO

Article history:
Received 15 March 2013
Received in revised form 4 June 2013
Accepted 4 June 2013
Available online 21 August 2013

Keywords:
Particle induced X-ray emission
X-ray production cross sections
ECPSSR
L-shell

ABSTRACT

The X-ray emissions induced by protons and alpha-particles of the elements Ag and Ru were measured on mono-elemental thin films. L-shell X-ray production cross sections were obtained for the three L-subshells, considering absorption corrections. The Ag X-ray production cross sections agree with experimental data of other authors and with theoretical models, and were used to endorse the quality of the experimental values for Ru, that were not found in the literature.

1. Introduction

The experimental confirmation of fundamental atomic parameters like the X-ray production cross section is of paramount importance for precise measurements in X-ray analysis, as for PIXE (induced either by protons or by alpha-particles), that has been used for trace analysis of many elements [1,2] in many different samples [1,3,4]. Empirical and semi-empirical expressions [5] have been developed to predict the values of the X-ray production cross sections of most elements, and theoretical models [6] are proposed to elucidate the mechanisms of particle–matter interaction. However the X-ray production cross section of some elements still needs experimental confirmation [7,8].

The ionization cross sections necessary for standardless analysis can be easily determined from the experimental X-ray production cross sections, once the fluorescence yields of the relaxation processes in the electronic distribution are known [9]. They are quite well established for K-shell ionizations of most elements, except for the very light ones. However, L-shell X-ray production cross sections are difficult to compare to the theoretical ionization cross sections, because of the intra-shell transitions [10], considering that the Coster–Kronig coefficients are known only with a large level of uncertainty.

There is no reliable theory that can predict L-shell ionization cross sections neither by proton nor by alpha-particle impact for all atomic numbers [8,11]. In addition, L-subshell X-ray production cross sections are poorly corroborated with experimental results for elements with atomic number below 45 [7,8,12]. Some elements require experimental support for their subshell X-ray production cross sections, particularly this is the case of Ru [7], even though total X-ray production cross sections have been determined [13]. This lack of data hampers the analysis of trace amounts of Ru in geological [2], medical [14], and technological [15] samples.

The quality of experimental data depends of the availability of good samples and reliable measuring devices. The development of ultra-high vacuum facilities for thin film preparation and a measuring setup with new detectors and faster electronics are expected to bring improvements to the dataset available for comparison. In thin films the calculations for X-ray production cross section is facilitated, due to the assumption of single interactions of the particles when impinging on the film.

Using the thin film approximation, the X-ray production cross section of each L subshell ($\sigma_{L_s}(E,A)$), as a function of energy (E) and type of incident particle (A) can be written as:

$$\sigma_{L_s}(E,A) = \sum_i \frac{Y_i(E,A)}{\varepsilon_i \varphi (Nt)} \quad (1)$$

where $Y_i(E,A)$ is the intensity of a L-shell X-ray line (i) that belongs to the subshell s, ε_i is the detector efficiency at this energy, φ is the total number of incident particles, and (Nt) is the number of target atoms per unit area.

* Corresponding author. Tel.: +55 51 33086539.
E-mail address: anapaula.bertol@gmail.com (A.P.L. Bertol).

0168-583X/$ - see front matter © 2013 Elsevier B.V. All rights reserved.
http://dx.doi.org/10.1016/j.nimb.2013.06.061

This work intends to contribute with new experimental data for L-subshell X-ray production cross sections induced by protons and alpha-particles in the 0.7–2.0 MeV/amu range for Ru and Ag.

2. Experimental

2.1. Sample preparation and characterization

10 nm films of Ru and Ag were deposited on vitreous carbon planchets (Ted Pella), by magnetron sputtering (AJA International ATC ORION 8 UHV), using ultrapure (99.999%) Ag and Ru targets.

The areal densities (*Nt*) were determined with Rutherford backscattering spectrometry (RBS) using 1 MeV alpha-particles in an ion accelerator (High Voltage Engineering, Tandetron 3MV). The SIMNRA [16] software was used to fit the experimental results. Ru and Ag film areal densities were 58.25 (0.17) $\times 10^{15}$ at/cm^2 and 47.12 (0.43) $\times 10^{15}$ at/cm^2, respectively.

2.2. PIXE measurements

The samples were irradiated with protons and alpha-particles in the 0.7–2.0 MeV/amu range. X-ray spectra were obtained with an EDX Si(Li) detector placed at 135° of the particle beam (e2 V Scientific Instruments, model Sirius 80, with 148 eV energy resolution at the Mn K_α line).

The Ag spectra were induced with proton energies of 0.7, 0.8, 0.9, 1.0, 1.2, 1.5, 1.8 and 2.0 MeV, and with alpha-particles with energies of 4.0, 5.0, 6.0 and 6.9 MeV (corresponding to 1.0, 1.25, 1.5 and 1.725 MeV/amu). The Ru spectra were induced with protons energies of 0.7, 0.8, 0.9, 1.0, 1.2 and 1.5 MeV and with the same alpha particle energies as Ag.

The spectra were charge normalized and fitted using a 9 Gaussian curve fit with the software Origin 6^{TM}.

2.3. EDX detector efficiency

The solid angle was determined from geometrical considerations, and the detector efficiency calculated from the product of the fraction of the solid angle and the absorption terms of the layers in front of the active volume in the Si(Li) detector, according to Eq. (2):

$$\varepsilon = \frac{\Omega}{4\pi}\exp[-\sum_{i=1}^{2}\mu_i x_i] \quad (2)$$

where $\Omega/4\pi$ is the solid angle subtended by the detector, μ_i is the absorption coefficient of each layer in front of the intrinsic volume, and x_i is the corresponding thickness. In this detector only the Be window and the Ni contact had to be considered, because it does not present a dead layer. The latter information, supplied by the manufacturer (personal communication, SGX Sensortech (MA) Ltd.) was confirmed by the bremsstrahlung measurements of a pure carbon planchet that showed no silicon edge jump, as was observed by Cohen [17] when using a Si(Li) detector with a dead layer. The detector efficiency was calculated using a sample-detector distance of 44.2(0.6) mm, exposed detector area of 63.6(0.1) mm^2, Be window thickness of 12.5(0.2) μm, and Ni contact thickness of 12(0.5) nm. The standard uncertainties in parenthesis were established from geometrical measurements, estimated mechanical precision of the turning lathe, and the last two from manufacturer information.

3. Results

Nine transitions were considered for the fittings: for the L_3-(L_{III}-M_I, $L_{III}M_{IV,V}$, $L_{III}N_{IV,V}$,), for the L_2-($L_{II}M_{IV}$, $L_{II}N_{IV}$, $L_{II}M_I$), and for the L_1-(L_IM_{II}, L_IM_{III}, $L_IN_{II,III}$) subshells.

The fittings of the Ag spectra were initialized with the nominal characteristic energy values [18] and the line widths were kept approximately at the value of the detector resolution. As can be ascertained by the residue plot in Fig. 1a, the Ag spectrum excited with 1.2 MeV protons adjusted well with Gaussian curves.

Due to the extreme overlap of the spectral lines, the fitting of the Ru spectra was only possible with the additional hypothesis that the line widths were similar to the corresponding ones in the Ag spectra. The initial values for the Ru-fit were taken from the Ag-fit and then released to vary, each at a time, until the chi-square achieved a minimum. The resulting fit and the residual plot are shown in Fig. 1b.

The X-ray production cross sections of each line were determined and added to their respective subshell L_1, L_2, and L_3. The results for Ag are shown in Fig. 2a and b, and for Ru in Fig. 2c and d, for proton and alpha-particle excitation, respectively. The bars cover a confidence interval of 68.27% [19].

The comparison of the total X-ray production cross-sections induced with protons obtained in this work with the experimental values from the literature is presented in Table 1. It can be seen, that the agreement is within the stated uncertainty with Sow [12] and Miranda [13] while the data of Reis [5] are lower. Our results of the partial X-ray production cross sections are presented as well, however are not compared with the literature, because of the choices of other authors to consider or not the spectral overlap of lines from different subshells (e.g. $L_{III}M_{IV,V}$ with $L_{II}M_I$ ($L_{\alpha_{1,2}}$ with L_η) or $L_{III}N_{IV,V}$ with L_IM_{III} (L_{β_2} with L_{β_3})).

The experimental X-ray production cross sections induced by alpha-particles for the L_1, L_2, L_3 subshells, and for L_{total} are presented in Table 2. In the literature the sparse experimental data for Ag excited with alpha-particles either are not in the same energy range [20] or present the data only in graphic form [21]. For Ru we could not find previous experimental data.

The theoretical values of X-ray production cross sections were obtained from the code ISICS 11 [22], which is a stand-alone package that uses Gauss–Legendre quadrature integration to obtain the form factors needed for the calculation of PWBA and ECPSSR K-, L-, and M-shell cross sections for any projectile/atom combination. The software uses the database of Krause [9] to convert theoretical ionization cross sections to X-ray production cross sections.

4. Discussion

Since ECPSSR seems to be more appropriate to describe our results (Fig. 2), the deviations were plotted as the ratio between

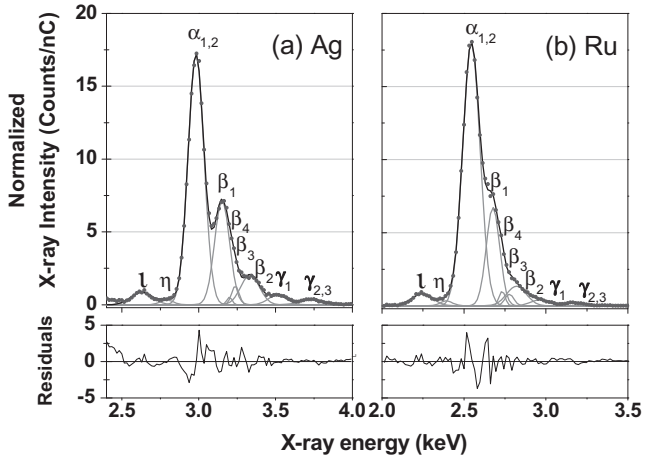

Fig. 1. Gaussian curve fitting of the (a) Ag spectrum (excited with 1.2 MeV protons) and (b) the Ru spectrum excited with 0.9 MeV protons. The residual plots are in standard deviation units.

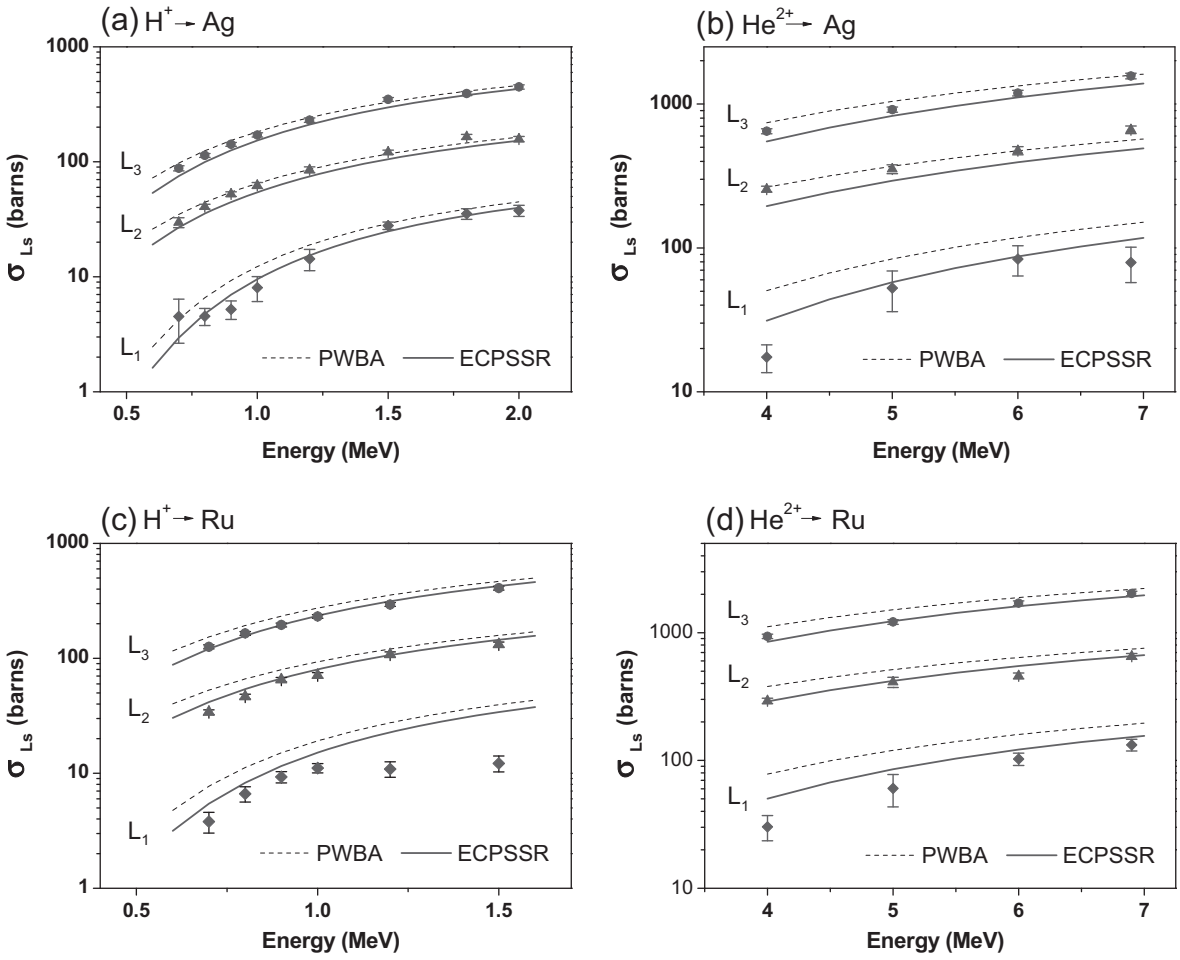

Fig. 2. X-ray production cross sections for the subshells L_1, L_2 and L_3 of Ag, induced with (a) protons, and (b) alpha-particles, and for the subshells L_1, L_2 and L_3 of Ru, induced with (c) protons, and (d) alpha-particles. The bars cover a confidence interval of 68.27%.

Table 1
Experimental proton induced X-ray production cross sections for Ag and Ru.

E (MeV)	L_1	L_2	L_3	L_{total}	L_{total}[12]	L_{total}[5]	L_{total}[13]
Ag							
0.7	4.5(1.9)[a]	29.7(2.9)	87.8(4.5)	122.0(9.3)	–	96.784	119(7.6)
0.8	4.5(0.8)	40.8(1.9)	113.7(4.5)	159.0(7.1)	156.151	128.117	
0.9	5.2(1.0)	52.4(2.4)	141.8(5.6)	199.4(9.0)	–	162.108	
1.0	8.1(2.0)	62.4(3.6)	171.3(7.3)	242(13)	254.7	197.55	
1.2	14.3(3.0)	85.2(5.2)	230(10)	330(18)	336.44	273.7	
1.5	27.9(2.1)	121.4(5.2)	349(13)	498(21)	–	391.67	
1.8	35.3(3.8)	164.9(7.8)	393(16)	593(27)	614.84	498.61	
2.0	37.7 (4.2)	157.5(8.4)	448(18)	643(31)	666.13	585.83	
Ru							
0.7	3.8(0.8)	34.1(1.6)	125.9(4.8)	163.8(7.2)	–	–	159(20)
0.8	6.6(1.0)	46.5(2.2)	164.7(6.5)	217.8(9.7)	–	–	
0.9	9.3(1.1)	65.2(2.9)	195.1(7.4)	270(11)	–	–	
1.0	11.1(1.0)	71.3(3.8)	231.5(8.7)	314(14)	–	–	
1.2	10.9 (1.7)	108.1(5.8)	294(11)	413(19)	–	–	
1.5	12.2(1.9)	131.9(6.5)	418(15)	552(24)	–	–	

[a] The values in parenthesis are the standard uncertainties.

experimental and calculated X-ray production cross section (Fig. 3). It can be observed that the best agreement occurs for the Ru-L_3 subshell, for protons and alpha-particles (Fig. 3a). For the Ag-L_3 subshell the experimental data are around 15% higher than the theory.

For the L_2 subshell (Fig. 3b), the experimental values for Ru are in good agreement with theory, except in the case of irradiation with protons at low energies. For the Ag-L_2 subshell our experimental values are about 15% (for protons) and 25% (for alpha-particles) above the theoretical values.

The results for the L_1-subshell show large uncertainties, because these lines have comparatively low intensities. For Ru the experimental values lie below the ECPSSR theory, but improve with increasing energy in the case of irradiation with alpha-particles.

Table 2
Experimental alpha-particle induced X-ray production cross sections for Ag and Ru.

E (Mev)	L_1	L_2	L_3	L_{total}
Ag				
4.0	17.4(3.8)	256(12)	647(26)	921(43)
5.0	53(17)	353(25)	914(38)	1320(80)
6.0	84(20)	475(31)	1193(55)	1751(106)
6.9	79(22)	663(40)	1569(71)	2311(132)
Ru				
4.0	30.3(6.7)	293(15)	935(38)	1258(59)
5.0	60(17)	411(38)	1215(51)	1686(106)
6.0	103(11)	458(24)	1700(69)	2261(105)
6.9	132(14)	653(34)	2025(81)	2810(129)

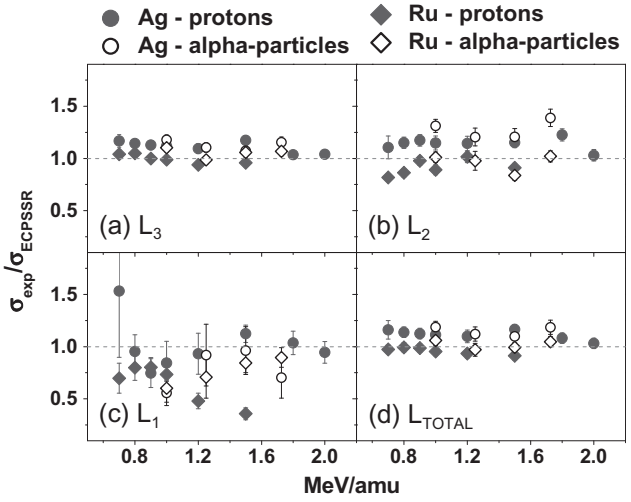

Fig. 3. Ratios of the experimental cross sections and the predictions of the ECPSSR theory for (a) L_3, (b) L_2, (c) L_1 subshells, and (d) total L-shell for Ag (circles) and Ru (diamonds), induced by protons (filled symbols) and alpha-particles (open symbols). The bars cover a confidence interval of 68.27%.

The Ag experimental data agree with the theory for both, proton and alpha-particles, within the large uncertainty.

The L_{total} production cross section for Ru (Fig. 3d) agrees very well with the theory. The results for L_{total} of Ag are around 15% above the values predicted by the theory (due to the values of the Ag-L_3-subshell, which is the main contribution to L_{total}).

Considering that the experimental data were obtained using the same procedures, the differences in their agreement with theory seem to lie outside the realms of experiment. The explanation could be the high uncertainties of the fluorescence yield of each sub-shell, stated to be in the 10–30% range for elements with $40 < Z < 50$ [9]. It has been pointed out [23] that the results of this conversion critically depend on the utilized database. The results are as well affected by multiple ionization [13], however the discussion about these effects transcends the scope of this article.

5. Conclusion

The X-ray production cross sections for the Ru and Ag L_1, L_2, and L_3-subshells for protons and alpha-particles were determined experimentally. The intensities of the Ru and Ag L-lines in the X-ray spectrum were fitted with 9 Gaussian curves. The values for Ag obtained in this work are in good agreement with the data reported by Sow [12], used as reference cross sections in the GUPIX database. Considering that the experimental procedures and data reduction were identical for Ru and Ag, the accuracy of the latter vouch for the reliability of the up to now unavailable experimental data of the Ru-L_1, -L_2 and -L_3 X-ray production cross sections.

For Ru the L_3 subshell the experimental values of the X-ray production cross sections showed excellent agreement with ECPSSR theory for both, protons and alpha-particles. For the Ru-L_2 subshell there was a good agreement with theory, except in the case for irradiation with protons at low energies. The experimental results of the Ru-L_1-subshell lie below the theoretical curve. However this deviation does not affect the total X-ray production cross section, and the obtained values agree with the theoretical predictions for protons as well as for alpha-particles.

Acknowledgments

The authors thank the Laboratório de Conformação Nanométrica (IF-UFRGS) for sample preparation and the Laboratório de Implantação Iônica (IF-UFRGS) for PIXE and RBS measurements. They also acknowledge financial support from the Brazilian funding agencies CAPES, CNPq and FAPERGS and from the Argentinean SPU/Ministerio de Educación.

References

[1] H.J. Annegarn, C.S. Erasmus, J.P.F. Sellschop, Nucl. Instrum. Methods Phys. Res., Sec. B 3 (1–3) (1984) 181.
[2] J.E. Mungall, D.R.A. Andrews, L.J. Cabri, P.J. Sylvester, M. Tubrett, Geochim. Cosmochim. Acta 69 (2005) 4349.
[3] L. Beck, X-Ray Spectrom. 34 (2005) 393.
[4] T. Dupuis, G. Chêne, F. Mathis, A. Marchal, M. Philippe, H.-P. Garnir, D. Strivay, Nucl. Instrum. Methods Phys. Res., Sect. B 268 (2010) 1911.
[5] M.A. Reis, A.P. Jesus, At. Data Nucl. Data Tables 63 (1996) 1.
[6] W. Brandt, G. Lapicki, Phys. Rev. A 23 (1981) 22.
[7] I. Orlic, C.H. Sow, S.M. Tang, At. Data Nucl. Data Tables 56 (1994) 159.
[8] G. Lapicki, Nucl. Instrum. Methods Phys. Res., Sect. B 189 (2002) 8.
[9] M.O. Krause, J. Phys. Chem. Ref. Data 8 (1979) 307.
[10] S. Puri, D. Mehta, B. Chand, S. Nirmal, J.H. Hubbell, P.N. Trehan, Nucl. Instrum. Methods Phys. Res., Sect. B 83 (1993) 21.
[11] J.L. Campbell, Th.L. Hopman, J.A. Maxwell, Z. Nejedly, Nucl. Instrum. Methods Phys. Res., Sect. B 170 (2000) 193.
[12] C.H. Sow, I. Orlic, T. Osipowicz, Nucl. Instrum. Methods Phys. Res., Sect. B 85 (1994) 133.
[13] J. Miranda, O.G. de Lucio, E.B. Téllez, J.N. Martínez, Rad. Phys. Chem. 69 (2004) 257.
[14] D.O. Boerna, E.P. Smit, N. Roosnek, Nucl. Instrum. Methods Phys. Res. Sect. B 36 (1989) 60.
[15] C. Bianchini, A. Meli, S. Moneti, F. Vizza, Organometallics 17 (1998) 2636.
[16] Mayer, SIMNRA User Guide Technical Report IPP 9/113, Max Planck Institut für Plasmaphysik, Garching, Germany, 1997.
[17] D.D. Cohen, E. Stelcer, R. Siegele, M. Ionescu, M. Prior, Nucl. Instrum. Methods Phys. Res., Sect. B 266 (2008) 1149.
[18] J.A. Bearden, Rev. Mod. Phys. 39 (1967) 78.
[19] B.N. Taylor, C.E. Kuyatt, Guideline 1297, Natl. Inst. Stand. Technol. (1994) .
[20] J. Braziewicz, E. Braziewicz, J. Ploskonka, M. Pajek, G.M. Osetynski, J. Phys. B 17 (1984) 3245.
[21] E. Perillo, G. Spadaccini, M. Vigilante, P. Cuzzocrea, J. Phys. B 19 (1986) 4161.
[22] S.J. Cipolla, Comp. Phys. Commun. 182 (2011) 2439.
[23] J. Miranda, C. Romo-Kröger, M. Lugo-Licona, Nucl. Instrum. Methods Phys. Res., Sect. B 189 (2002) 21.